

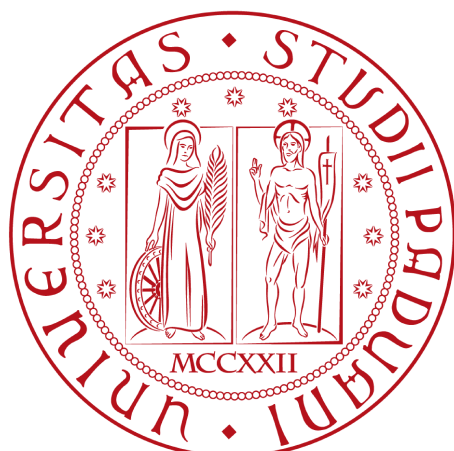
MATTEO ABIS

A SEARCH FOR EXOTIC PARTICLES OF CHARGE  $5/3$   
WITH THE CMS DETECTOR



A SEARCH FOR EXOTIC PARTICLES OF CHARGE  $5/3$  WITH THE  
CMS DETECTOR

MATTEO ABIS



Dipartimento di Fisica e Astronomia  
Università degli Studi di Padova

A.A. 2011/2012

Matteo Abis: *A search for exotic particles of charge 5/3 with the CMS detector*, © A.A. 2011/2012

*Ohana* means family.  
Family means nobody gets left behind, or forgotten.  
— Lilo & Stitch

Dedicated to the loving memory of Rudolf Miede.

1939 – 2005



## ABSTRACT

---

Short summary of the contents in English...

## ZUSAMMENFASSUNG

---

Kurze Zusammenfassung des Inhaltes in deutscher Sprache...



## ACKNOWLEDGMENTS

---

Put your acknowledgments here.

Many thanks to everybody who already sent me a postcard!

Regarding the typography and other help, many thanks go to Marco Kuhlmann, Philipp Lehman, Lothar Schlesier, Jim Young, Lorenzo Pantieri and Enrico Gregorio<sup>1</sup>, Jörg Sommer, Joachim Köstler, Daniel Gottschlag, Denis Aydin, Paride Legovini, Steffen Prochnow, Nicolas Repp, Hinrich Harms, Roland Winkler, and the whole L<sup>A</sup>T<sub>E</sub>X-community for support, ideas and some great software.

*Regarding LyX:* The LyX port was initially done by Nicholas Mariette in March 2009 and continued by Ivo Pletikosić in 2011. Thank you very much for your work and the contributions to the original style.

---

<sup>1</sup> Members of GuIT (Gruppo Italiano Utilizzatori di T<sub>E</sub>X e L<sup>A</sup>T<sub>E</sub>X)



## CONTENTS

---

1	THE THEORY OF THE TOP PARTNERS	1
1.1	The Standard Model	1
1.1.1	The unbroken SM	1
1.1.2	Spontaneous symmetry breaking: the Higgs mechanism	2
1.1.3	The hierarchy problem	3
1.1.4	The top partners	3
2	THE LHC AND THE CMS DETECTOR	5
2.1	The Large Hadron Collider	5
2.2	The Compact Muon Solenoid	5
2.2.1	Coordinate convention	6
2.2.2	Structure of the detector	6
2.2.3	The tracking system	7
2.2.4	The electromagnetic calorimeter	8
2.2.5	The hadron calorimeter	9
2.2.6	The muon detectors	9
2.2.7	The trigger and data acquisition system	9
3	SIMULATION, RECONSTRUCTION AND DATASETS	11
3.1	Simulation	11
3.2	The reconstruction of physics objects	12
3.2.1	Muon reconstruction	13
3.2.2	Electron reconstruction	14
	BIBLIOGRAPHY	17

## LIST OF FIGURES

---

Figure 1	The particles in the unbroken SM.	2
Figure 2	Radiative correction to the Higgs mass from the top quark.	3
Figure 3	Typical single and pair production the top part- ner $T_{5/3}$ at the LHC.	4
Figure 4	A view of the LHC and the four experiments.	6
Figure 5	The CMS detector.	6
Figure 6	Transverse view of the CMS detector with some examples of tracks.	7
Figure 7	Energy resolution of the ECAL as measured in $Z \rightarrow ee$ events in the 2011 data.	8
Figure 8	The layout of the muon detectors.	9
Figure 9	Muon momentum resolution as a function of $p_T$ in regions with different pseudorapidity. The blue squares are for the muon system only, the green circles for the inner tracker only, and the red circles for the combined reconstruction	13
Figure 10	Illustration of the isolation observable.	14
Figure 11	An illustration of the <i>bremsstrahlung</i> recovery algorithm.	15

## LIST OF TABLES

---

## LISTINGS

---

## ACRONYMS

---

## THE THEORY OF THE TOP PARTNERS

---

### 1.1 THE STANDARD MODEL

The SM is a quantum field theory developed in the 1970s. It describes matter and the electromagnetic, weak and strong nuclear forces in terms of point-like particles.

The most profound insight in the SM is that all of these interactions are determined by symmetry principles, called local gauge symmetries. This idea is connected with the fact that the conserved physical quantities, e.g. electric charge, are conserved at every point in space-time, and not just globally. This connection is given by Nöther's theorem in the lagrangian formalism.

The treatment of one particular property of the particles requires some ingenuity. Mass terms are not allowed in the SM lagrangian, because they break the fundamental symmetry principles. Yet it is obvious from observation that most particles have mass. The Higgs mechanism with spontaneous symmetry breaking was devised to solve this problem, and appears to be close to experimental confirmation at the time of writing.

We will first review the features of the unbroken SM, then introduce the Higgs field and finally present some shortcomings of this theoretical description.

A complete description can be found elsewhere, the following section will highlight the material that is relevant to the problems we are investigating in the rest of our work.

#### 1.1.1 *The unbroken SM*

All of the matter particles in the SM are fermions, and are usually divided in two categories: particles that feel the strong force, called *quarks*, and particles that do not, called *leptons*. Quarks and leptons are grouped into three *families* or *generations*. Particles from different generations have exactly the same properties, except for mass. The origin of this family structure is still unknown.

A force is introduced by requiring the lagrangian for the matter fields to be invariant under a group of space-time dependent transformations, called *gauge* transformations.

The theory of QED was the first successful gauge theory. It describes the electromagnetic force, with a U(1) gauge invariance. As a consequence, a *gauge boson* has to be introduced to preserve the local symmetry, that is the photon.

The electromagnetic and weak forces are then unified by a gauge group  $SU(2)_L \times U(1)_Y$ , with the L subscript denoting the fact that the  $SU(2)$  gauge transformations only involve the left-handed fermions. The Y subscript is intended to indicate that this  $U(1)_Y$  group is not the same as the aforementioned group for QED. The number of gauge bosons must be the same as the dimension of the gauge group, so that we now get four vector bosons: the photon, the  $W^\pm$  and the Z.

The description of the strong force involves the group  $SU(3)$ . The charge of the strong force is called *colour*, it is carried by eight bosons called *gluons*. Figure 1 summarizes the particle contents of the unbroken SM.

Three Generations of Matter (Fermions)			
	I	II	III
mass→	2.4 MeV	1.27 GeV	171.2 GeV
charge→	$\frac{2}{3}$	$\frac{2}{3}$	$\frac{2}{3}$
spin→	$\frac{1}{2}$	$\frac{1}{2}$	$\frac{1}{2}$
name→	u up	c charm	t top
	d down	s strange	b bottom
	v <sub>e</sub> electron neutrino	v <sub>μ</sub> muon neutrino	v <sub>τ</sub> tau neutrino
	e electron	μ muon	τ tau
Bosons (Forces)			
	γ photon	g gluon	Z <sup>0</sup> weak force
	W <sup>±</sup> weak force		

Figure 1: The particles in the unbroken SM.

### 1.1.2 Spontaneous symmetry breaking: the Higgs mechanism

We have only considered massless particles. This is not the case for all the known fermions, and for the W and Z bosons. A mechanism was proposed to preserve the gauge invariance of the lagrangian, while the vacuum state is no longer a singlet under the action of the gauge group.

Spontaneous symmetry breaking of the local gauge symmetry in the SM provides massive W and Z bosons and a new boson, called the Higgs boson. In addition, we can obtain massive fermions by coupling them to the Higgs field with Yukawa terms.

### 1.1.3 The hierarchy problem

Recently found evidence for a light Higgs boson, with a mass near 125 GeV, are thought to be an indication of new symmetries and new particles beyond the SM.

The theory predicts that the mass  $m_H$  is subject to large radiative corrections from loop diagrams similar to figure 2, that should increase it by a large amount. In the SM, fine tuning is required to prevent this corrections from becoming too large. Theoretical physicists generally dislike this fine tuning on grounds of *naturalness*.

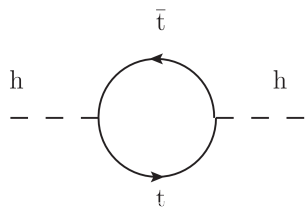


Figure 2: Radiative correction to the Higgs mass from the top quark.

The most notorious example of an extension to the SM that can eliminate this naturalness problem is supersymmetry, where the radiative corrections to the Higgs mass of the SM fermions are canceled by the contributions from their superpartners.

There exist many theories that do not invoke supersymmetry as the solution to the hierarchy problem. A robust and generic prediction of many of them is the existence of new particles, the top partners, again balancing the largest contribution to  $m_H$  coming from the top quark.

### 1.1.4 The top partners

Theoretical developments predicting the existence of top partners stem from the search for a way of introducing gravity in the SM, while solving the hierarchy problem at the same time.

Five-dimensional space-time theories including gravity can be formulated in terms of effective 4-d lagrangians where SM quarks mix with the top partners, which, again from arguments of naturalness, should have a mass below or slightly above the TeV scale. The lightest quarks have a small mass, indicating that their mixing with the new particles is negligible. The top quark, having a very large mass, should have a sizeable mixing with its partner, possibly making deviation from the SM top interactions detectable at the LHC.

We use the top partner model from [8] to describe our signal, with vertices with the vector bosons and the top quark. We study the possibility of observing the top partners in the very clean channel of two

same-sign hard leptons. Typical production and decay diagrams are shown in figure 3.

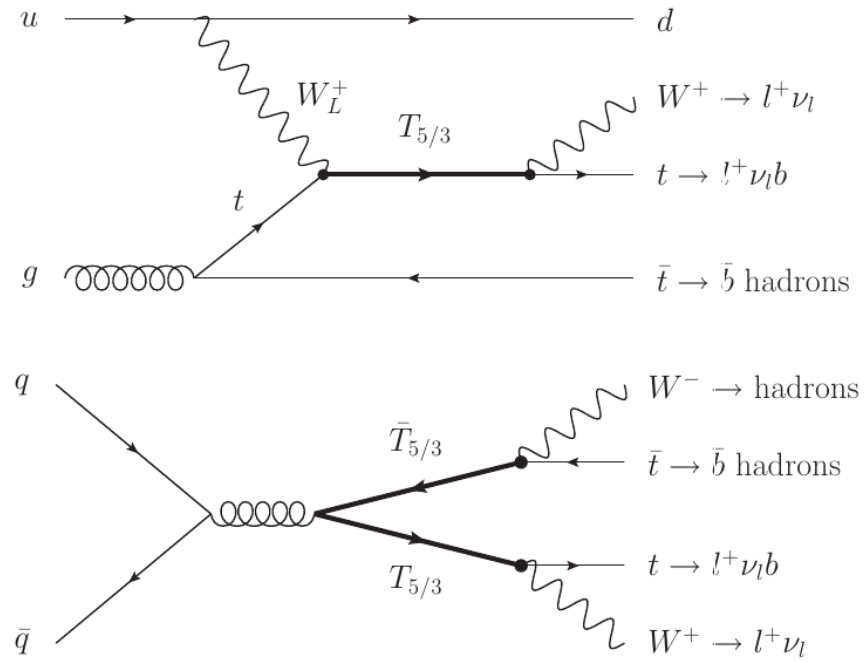


Figure 3: Typical single and pair production the top partner  $T_{5/3}$  at the LHC.

# 2

## THE LHC AND THE CMS DETECTOR

---

### 2.1 THE LARGE HADRON COLLIDER

The LHC is a ring-shaped proton-proton accelerator with a circumference of 27 km. It is hosted in a tunnel 45 to 170 m below ground at the CERN laboratory in Geneva, Switzerland. In 2011, the LHC accelerated two proton beams up to an energy of 3.5 TeV each and an instantaneous luminosity of up to  $3.55 \cdot 10^{33} \text{ cm}^{-2}\text{s}^{-1}$ .

The two proton beams are pre-accelerated through four smaller systems before being injected in the LHC:

- the linear accelerator (up to 50 MeV)
- the proton synchrotron booster (up to 1.4 GeV)
- the proton synchrotron (up to 26 GeV)
- the super proton synchrotron (up to 450 GeV)

The protons travel in ultra-high vacuum around  $10^{-10}$  mbar, while different sets of magnets keep them in a circular orbit and provide acceleration and focusing.

Radio frequency cavities in the LHC accelerate the protons, providing an energy increase of 0.5 MeV/turn. Superconducting dipole magnets operate at currents of 11850 A to bend the trajectories of the protons with a magnetic field up to 8.3 T. Quadrupole magnets are employed to focus the beams, thus increasing the probability of an interaction when they collide. The magnets are cooled with superfluid helium at 1.9 K. The beams are made of “bunches” of protons with a time spacing of 75 ns.

At four different interaction points, the two proton beams are brought to collision where the experiments are located: CMS, ATLAS, LHCb and ALICE, as shown in figure 4. The first two are general purpose detectors. LHCb is designed for the study of CP violation in b physics, and ALICE for the analysis of the quark-gluon plasma produced mainly in heavy ion collisions.

### 2.2 THE COMPACT MUON SOLENOID

CMS is a general purpose detector based on interlocking cylindrical subdetectors in the central *barrel* region, closed by two *endcaps*, all placed coaxially with the beam and centred on the beam interaction point.



Figure 4: A view of the LHC and the four experiments.

### 2.2.1 Coordinate convention

The conventional coordinate system has its origin at the nominal interaction point. The  $z$  axis points along the beam direction, the  $y$  axis points vertically upwards, and the  $x$  axis points towards the centre of the LHC circumference. The  $xy$  plane is thus called the *transverse* plane as it is orthogonal to the CMS cylinder.

We define two angles in the transverse plane: the azimuthal  $\varphi$  angle is measured from the  $x$  axis, and the polar angle  $\theta$ , measured from the  $z$  axis. *Pseudorapidity* is defined as  $\eta = -\log \tan \theta/2$ .

### 2.2.2 Structure of the detector

A global view and a transverse section of the detector are shown in figures 5 and 6.

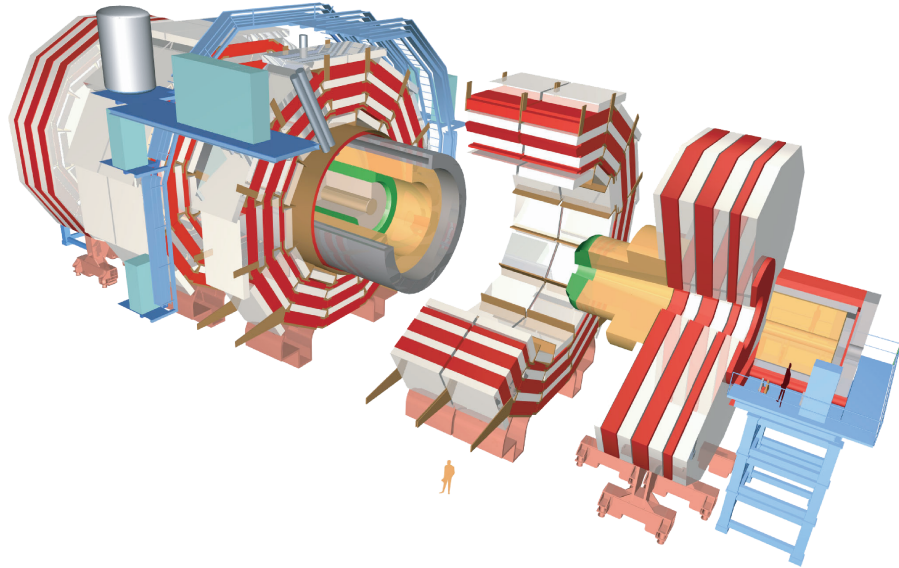


Figure 5: The CMS detector.

A superconducting solenoid 13.5 m and with a diameter of 5.9 m provides a uniform, axial magnetic field of 3.8 T. The return field sat-

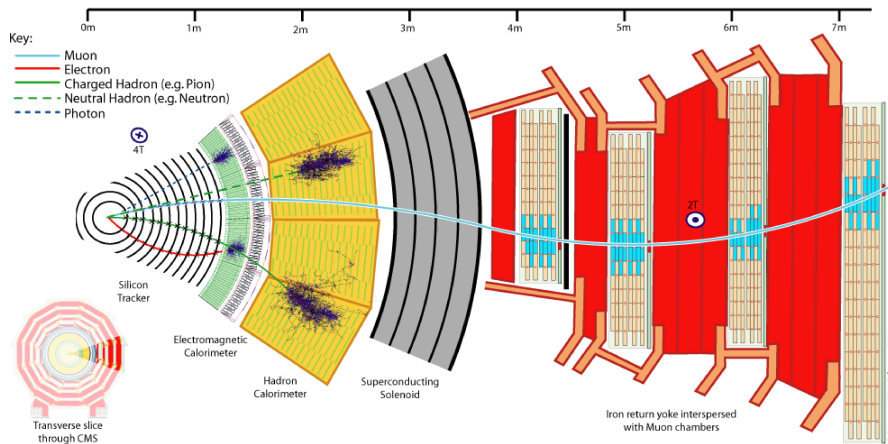


Figure 6: Transverse view of the CMS detector with some examples of tracks.

urates an iron yoke, which consists of five wheels in the barrel region and three disks in each of the two endcaps. Muon detectors are installed in the return yokes, with four stations of aluminium drift tubes in the barrel and cathode strip chambers with resistive plate chambers in the endcap.

The tracking system and the calorimeters are installed inside the solenoid. The tracker is a cylinder with a diameter of 2.6 m with three layers of pixel detectors, allowing exceptional measurements of the impact parameter of the particles and secondary vertex reconstruction, and ten layers of silicon microstrip detectors. The tracking system is surrounded by the calorimeters, which cover the region with  $|\eta| < 3$ . There is an electromagnetic calorimeter (ECAL), made of lead tungstate crystals and a brass/scintillator hadron calorimeter (HCAL). A forward calorimeter provides additional coverage up to  $|\eta| < 5$ .

### 2.2.3 The tracking system

Very high granularity and time resolutions are needed in the tough environment of the LHC experiments, with thousands of particles produced for every interaction. The high spatial resolution is particularly important in the region close to the primary interaction.

For these reasons, silicon detectors were chosen for the whole tracking system of the CMS experiment.

**THE PIXEL DETECTOR** is made of three cylinders in the barrel and two disks in each of the two endcaps. The spatial resolution on each hit is about  $10 \mu\text{m}$  in  $r\phi$  and about  $20 \mu\text{m}$  in  $z$ .

THE MICROSTRIP DETECTOR is made of concentrical layers in the barrel region, divided in two systems: the *tracker inner barrel* (TIB) and the *tracker outer barrel* (TOB).

The TIB has four layers in the region with  $20\text{ cm} < r < 55\text{ cm}$  and  $|z| < 65\text{ cm}$ . The sensors are  $10\text{ cm}$  long in  $z$ ,  $80$  to  $120\text{ }\mu\text{m}$  wide and  $320\text{ }\mu\text{m}$  thick. The single hit resolution is between  $23$  and  $34\text{ }\mu\text{m}$  in the  $r\text{-}\varphi$  plane, and about  $230\text{ }\mu\text{m}$  in  $z$ .

The TOB module is made of six layers, covering  $55\text{ cm} < r < 116\text{ cm}$  and  $|z| < 116\text{ cm}$ . The sensors have a length of  $25\text{ cm}$ , a width of  $180\text{ }\mu\text{m}$  and a thickness of  $500\text{ }\mu\text{m}$ . The single hit resolution is  $35$  to  $52\text{ }\mu\text{m}$  in the  $r\text{-}\varphi$  coordinates, and  $530\text{ }\mu\text{m}$  in  $z$ .

Two more modules are installed in the endcaps, arranged around the beam line: the *tracker inner disks* (TID) and *tracker outer endcaps* (TEC)

Each TEC module consists of nine disks, while the TID have three smaller disks. Both these modules have strips pointing radially toward the beam line with a thickness of  $320\text{ }\mu\text{m}$  to  $500\text{ }\mu\text{m}$ .

#### 2.2.4 The electromagnetic calorimeter

The ECAL is the inner calorimeter, made of  $61200$  lead tungstate crystals in the barrel and  $7324$  crystals in the endcaps. The base of the crystals is about  $2 \times 2\text{ cm}$  in size, with a depth of  $23\text{ cm}$ , corresponding to  $25$  radiation lengths.

The scintillation light is collected by avalanche photodiodes in the barrel and vacuum phototriodes in the endcaps. They have a high gain and are insensitive to the magnetic field of the detector.

The energy resolution of the calorimeter has been measured in  $Z \rightarrow ee$  events from the 2011 data [6], as shown in figure 7.

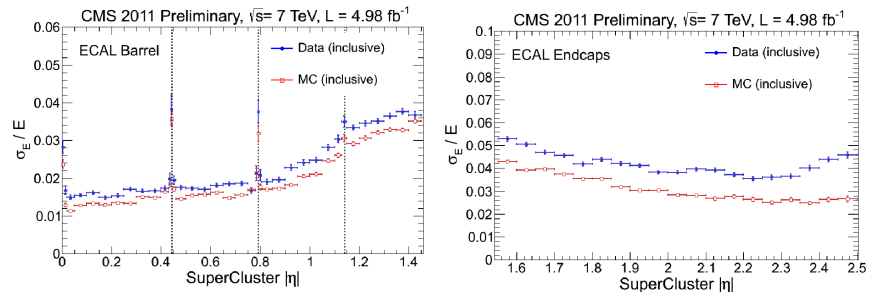


Figure 7: Energy resolution of the ECAL as measured in  $Z \rightarrow ee$  events in the 2011 data.

### 2.2.5 The hadron calorimeter

The HCAL surrounds the ECAL and is made of plastic scintillators interleaved with brass layers. It is composed of a *hadron barrel* up to  $|\eta| < 1.4$ , a *hadron endcap* for  $1.3 < |\eta| < 3.0$ . Two more systems provide very good hermeticity: the *hadron outer calorimeter* is placed outside the magnet in order to measure the energy of penetrating hadrons, while the *hadron forward calorimeter* extends the coverage up to  $|\eta| < 5$ .

### 2.2.6 The muon detectors

The muon system is installed in the return yokes of the magnet. Concentrical cylinders cover the barrel region up to  $|\eta| < 1.2$ , while four disks make up the endcap detectors ( $|\eta| < 2.4$ ). Three kind of gas detectors are employed: drift tubes in the barrel, cathode strip chambers id the endcaps, and resistive plate chambers in both. This last kind of detector has a fast response and is the most important for the trigger.

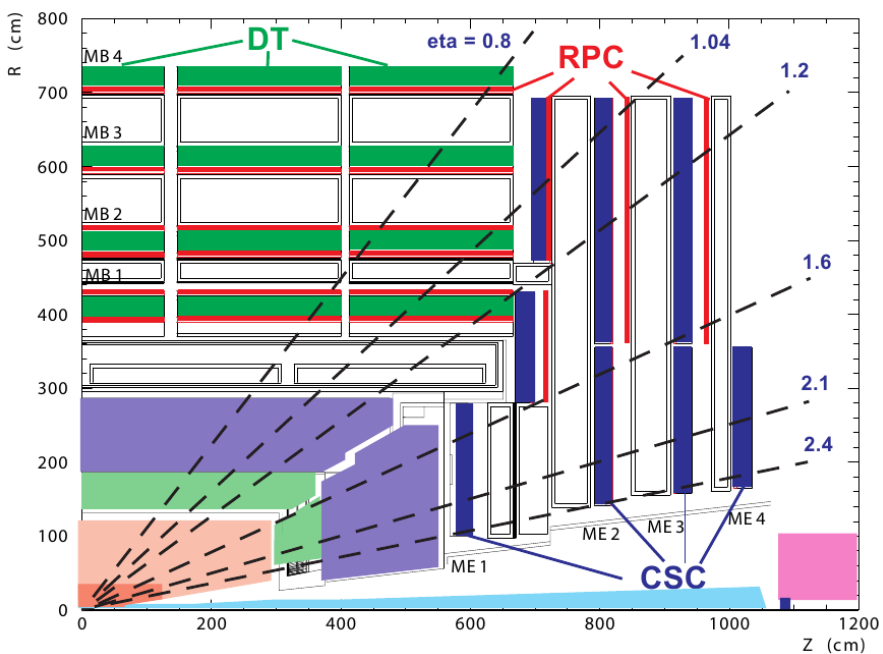


Figure 8: The layout of the muon detectors.

### 2.2.7 The trigger and data acquisition system

The design bunch spacing of the LHC is 25 ns, i.e. 40 MHz. About 100 interactions per second can be stored, so that the trigger has to provide a reduction factor of the order of  $10^5$ . The trigger system has two levels of selection: the *level 1* (L1) and the *high level trigger*.

**L1** is a hardware trigger, made of processors close to the detector components. It exploits coarse granularity information from calorimeters and muon chambers to identify electromagnetic clusters, muons, jets and missing  $E_t$ . Its processing time per event is on the order of a microsecond. It reduces the rate of events to less than 100 kHz.

**HLT** is a software trigger run on a farm of commercial CPUs, and has access to all event data, allowing for precise object reconstruction and energy/momentum evaluation. The HLT processing time is around 0.1 s per event.

# 3

## SIMULATION, RECONSTRUCTION AND DATASETS

---

### 3.1 SIMULATION

Accurate Monte Carlo simulations are needed in order to make sense of the data and search for new physics phenomena. The physics of the collisions is simulated by the event generators MadGraph [?] and PYTHIA [10]. Then, the propagation of the particles in the detector has to be worked out. Two different types of simulation are used by the CMS collaboration: a GEANT4-based [7] simulation, known as the *Full Simulation*, and a detector model with simplified geometry, response evaluation and pattern recognition to decrease the processing time per event, the *Fast Simulation* [4]. Both the FullSim and the Fast-Sim were employed in the generation of the background samples for our studies.

In the FullSim, the energy depositions in the sensitive detector volumes are converted to electronic signals using algorithms based on the observed detector behavior, including the simulation of electronics noise and cross-talk. In many cases, the simulated electronic parameters are identical to those of the real electronics; the constants specifying performance, calibrations, and noise behavior can be read from the same database used for the reconstruction of the real collision data. The output of this stage is simulated data in a format identical to that of the real raw data read from the detector. Further processing uses this data to simulate the formation of the L1 and HLT decisions using the same algorithms implemented online in the CMS trigger system. The simulated raw data that is produced is processed in a manner identical to that of the real data from LHC collisions.

The FastSim makes a number of approximations:

**CMS GEOMETRY:** the FastSim describes the detector with a simplified geometry of nested cylindrical layers. The particles are propagated from one layer to the next.

**MATERIAL EFFECTS:** five effects are taken into account. These are *bremsstrahlung*, photon conversion, multiple Coulomb scattering, energy loss through ionization and nuclear interactions. All of these are calculated analytically, except for nuclear interactions, since no analytical description is sufficient to describe the effect. Cross sections are taken from the PDG and the kinematics are derived from single particle collisions saved beforehand.

**TRACK RECONSTRUCTION:** the reconstruction is not usually part of the simulation. The FastSim includes it because, given the low

fake rate in the reconstruction, it is possible to emulate it at a lower computational cost. Only the hits of the simulated track are used to make a track candidate.

**MUONS:** muons are propagated through the tracker and calorimeters with average energy loss, then  $dE/dx$  and multiple scattering in the iron yokes of the muon chambers are computed. Muon simulated hits are produced in all sections of the muon systems.

**CALORIMETERS:** electron showers in the ECAL are simulated with the Grindhammer [9] parametrization. Photons undergo pair conversions based on the number of radiation lengths they have traversed. Detector effects such as energy leakage into the crystal gaps and into the HCAL are included, as well as electronic noise. Shower simulation in the HCAL is similar, with different types of particles parametrized from FullSim results.

### 3.2 THE RECONSTRUCTION OF PHYSICS OBJECTS

The particle flow [5] (PF) event reconstruction aims at reconstructing and identifying all stable particles in the event. The essential idea is to analyse the event combining the information from all the available subdetectors in an optimal way.

The CMS detector, with its large silicon tracker and its extremely precise electromagnetic calorimeter, appears to be ideally suited for this purpose. The fundamental building bricks of the PF reconstruction are charged particle tracks, ECAL and HCAL clusters and muon tracks. These must be delivered with a high efficiency and low fake rate even in high-density environments like jets. A jet is a collection of particles resulting from the decay of a quark or gluon and emitted in the direction of the primary particle.

Reconsider the design of the detector in figure 6. The logic you use to interpret this diagram is akin to that employed by the PF. An ECAL cluster not linked to any track is a photon, an ECAL and HCAL cluster matched to a track gives a charged hadron, while an HCAL cluster without a track identifies a neutral hadron. Electrons are basically ECAL-only clusters linked to a track. Muons are by far the easiest particles to recognize.

From these basic elements, composite objects can be reconstructed, such as  $\tau$  leptons from their decay products, jets and missing transverse energy from all the particles in the event.

Quality requirements are needed in the reconstruction of the physics objects: thousands of particles are created in each event and their tracks can overlap. The quality selections are the result of detailed studies by the CMS collaboration, aiming for the best compromise between purity and efficiency. These recommendations are described in the following paragraphs.

### 3.2.1 Muon reconstruction

Muons are not stopped inside the CMS detector and leave only a tiny fraction of their energy in the calorimeters. The information from the tracking system and the muon chambers is exploited for their reconstruction. The two systems are used independently in a first phase, where two algorithms are used:

**THE GLOBAL MUON RECONSTRUCTION**, or the *outside-in* approach, starts from a segment in the drift tubes or cathode strip chambers and extrapolates the seed layer by layer up to the tracker. If a matching track is found in the tracking system, the information from both tracks is combined to improve the resolution.

**THE TRACKER MUON RECONSTRUCTION**, or the *inside-out* method, extrapolates a track from the inner system to the muon chambers. The small energy loss due to interactions with the material of the magnets and calorimeters is taken into account, as well as an uncertainty arising from the possibility of multiple scattering.

The recommended selection requires these two algorithms to agree, as this improves the resolution for high- $p_T$  muons (figure 9).

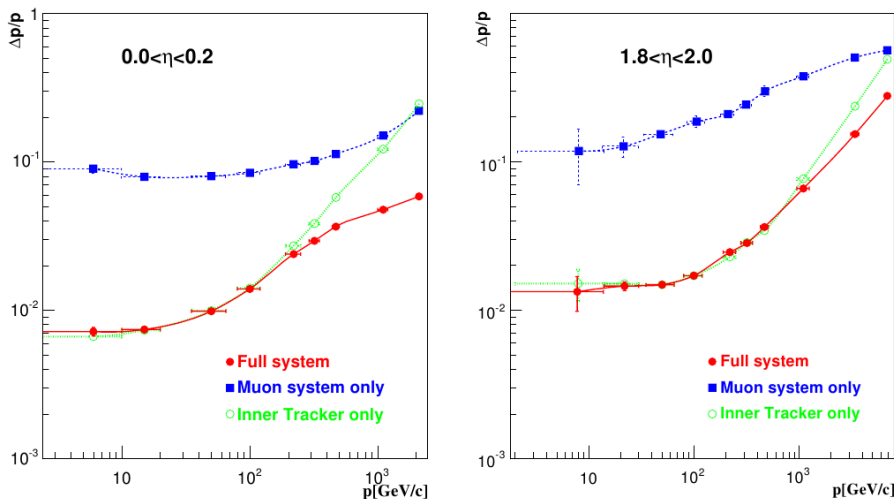


Figure 9: Muon momentum resolution as a function of  $p_T$  in regions with different pseudorapidity. The blue squares are for the muon system only, the green circles for the inner tracker only, and the red circles for the combined reconstruction

One of the most important observables for the muon candidates is the *relative isolation*. It indicates the amount of energy collected in the vicinity of the muon, by summing the contributions from the tracking system, the ECAL and the HCAL, divided by the  $p_T$  of the muon. The sum runs over all deposits within a cone of radius  $\Delta R = 0.3$  centred on the muon track, as illustrated in figure 10.

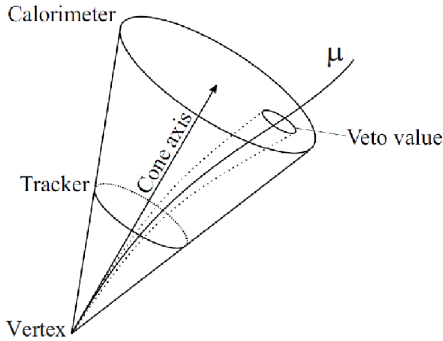


Figure 10: Illustration of the isolation observable.

### 3.2.2 Electron reconstruction

The tracks in CMS are reconstructed assuming that the particle is a muon. Coulomb scattering is the dominant effect on muons crossing material and its impact is modelled by gaussian fluctuations. This approach fails with electrons because of the highly non-gaussian *bremsstrahlung* emission. A customized track reconstruction was developed for electrons, where the hits are fitted using a *gaussian sum filter* (GSF) [3], i. e. the *bremsstrahlung* emission is modelled by a superposition of gaussian functions. However, this more sophisticated analysis demands more CPU power, at the order of a few hundreds milliseconds per track, and can be run only on a limited number of seeds.

The standard strategy to seed GSF tracks, hereafter called ECAL-driven seeding, heavily relies on the ability to gather into one single *supercluster* the entire energy deposit of the electron. The algorithm consists of three steps. First, cluster seeds are identified as local energy maxima above a given energy. Secondly, the seeds are grown by connecting cells with at least one side in common with a cell already in the cluster, and with an energy in excess of a given threshold. These thresholds are equivalent to two standard deviations of the electronic noise in the calorimeter, that is 80 MeV in the ECAL barrel, up to 800 MeV in the HCAL. Finally cluster energies and positions are determined from those clusters.

This implies collecting the electron and the *bremsstrahlung* photons energy deposits, which leads to clusters very extended along the azimuthal direction. This approach, which is efficient for isolated and high  $p_T$  electrons has unfortunately a limited efficiency in jets because the super-cluster collects additional contributions from other particles.

In contrast with this ECAL-driven approach, the strategy developed for the Particle Flow [2] starts from the tracks and can be explained with two extreme examples. When the *bremsstrahlung* emission is negligible, the electron trajectory is determined with good precision by the standard tracking algorithm, and the track can be reconstructed

up to the ECAL internal surface where it can be matched with the closest cluster. The momentum of the track can then be compared with the corresponding cluster energy, forming the  $E/p$  observable. If it is close to unity the track is selected to be then re-reconstructed with the GSF algorithm. On the contrary, if the electron loses a substantial fraction of its energy by *bremstrahlung* emission, the characteristics of the track are exploited. Indeed, either the pattern recognition manages to accommodate for the changes of curvature, and the fitted track  $\chi^2$  is usually large, or it cannot follow the electron trajectory and the track is short. Electron tracks are then selected based on the attempt made by the standard algorithm to reconstruct it.

The tracker-driven seeding developed for the PF reaches a 80% efficiency in the barrel with a 10% probability to select wrongly a pion, with an acceptable CPU consumption; a more sophisticated treatment described below is further applied to reject fakes at the final identification level. In addition, this new algorithm improves the overall seeding efficiencies for isolated electron in CMS by 15% at 5 GeV with respect to the standard ECAL-driven seeding.

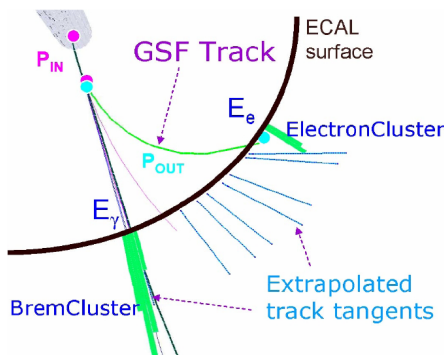


Figure 11: An illustration of the *bremstrahlung* recovery algorithm.

The procedure to collect all the calorimeter energy deposits, i.e., the *bremstrahlung* recovery, is driven by the GSF track (figure 11). For each tracker layer, where the material is mainly localized, a *bremstrahlung* photon emission is sought by computing a straight-line extrapolation, tangent to the track, up to the ECAL. If it matches a cluster, not already linked to a track, this cluster is selected as part of the electron. This procedure allows between 96% and 99% of the energy deposited in the ECAL to be collected.

The relative isolation is defined with the same method already described for the muons.

The charge of the electrons can be measured in three ways:

**THE GSF TRACK**, whose curvature in the magnetic field of the detector defines the sign of the charge of the electron.

**THE CTF TRACK**. Another algorithm for the reconstruction of the tracks. It accounts for multiple scattering with Kalman filter

techniques [1]. The curvature of this track is another measurement of the charge.

**SUPERCLUSTER POSITION** : the relative position of the track seed and the largest deposition in the ECAL provides an independent estimate of the electric charge.

Requiring these three methods to agree strongly decreases the probability of a charge mismeasurement. This is particularly important for our analysis, since the production of opposite-sign electrons is very abundant in Standard Model processes, and the accurate identification of the charge of the electrons almost eliminates these contributions to our selection.

Electrons can also be created from the conversion of an energetic photon. These are rejected if one of the following occurs:

**AT LEAST ONE MISSING HIT** in the tracker. Photons are neutral, so they usually miss hits in one or more layers.

**TRACK DISTANCE**  $< 0.02$  cm. An electron coming from a conversion has a partner positron track. If an oppositely charged track is found within this distance, the electron is rejected.

$\Delta \cot \theta < 0.02$ . A geometrical variable also related to the partner track:  $\theta$  is the angle between the two tracks in the  $yz$  plane.

## BIBLIOGRAPHY

---

- [1] S. Baffioni, C. Charlot, F. Ferri, D. Futyan, P. Meridiani, I. Puljak, C. Rovelli, R. Salerno, and Y. Sirois. Electron reconstruction in cms. *The European Physical Journal C - Particles and Fields*, 49:1099–1116, 2007. ISSN 1434-6044. URL <http://dx.doi.org/10.1140/epjc/s10052-006-0175-5>.
- [2] F. Beaudette, D. Benedetti, P. Janot, and M. Pioppi. Electron reconstruction within the particle flow algorithm. *CMS Analysis Note*, (AN-2010/034), 2010.
- [3] CMS Collaboration. Reconstruction of electron tracks with the Gaussian-Sum Filter in the CMS tracker at LHC. *CMS Analysis Note*, (RN-2003-001), 2003.
- [4] CMS Collaboration. Fast simulation of the CMS detector. *Journal of Physics, Conference Series*, (219), 2010.
- [5] CMS Collaboration. Particle flow event reconstruction in CMS and performance for jets, taus and  $E_T^{\text{miss}}$ . *CMS Physics Analysis Summary*, (PFT-9-001), 2010.
- [6] The CMS collaboration. ECAL detector performance, 2011 data. May 2012.
- [7] GEANT4 Collaboration. GEANT 4 — a simulation toolkit. *Nucl. Instrum. Meth.*, (056), 2003.
- [8] Jan Mrazek and Andrea Wulzer. A Strong Sector at the LHC: Top Partners in Same-Sign Dileptons. *Phys.Rev.*, D81:075006, 2010. doi: 10.1103/PhysRevD.81.075006.
- [9] M. Rudowicz and S. Peters. Grindhammer G. *Nucl. Instrum. Meth. A*, (290):469, 1990.
- [10] T. Sjostrand, S.Mrenna, and P.Z.Skands. PYTHIA 6.4 physics and manual. *JHEP*, (05-026), 2006.